ChemPubSoc Europe

DOI: 10.1002/cphc.201300793

High-Temperature Elastic Moduli of Flux-Grown α-GeO_2 Single Crystal

Adrien Lignie,[a] Wei Zhou,[b] Pascale Armand,*[a] Benoit Rufflé,[b] Richard Mayet,[d] Jerôme Debray,[c] Patrick Hermet,[a] Bertrand Ménaert,[c] Philippe Thomas,[d] and Philippe Papet[a]

From high-precision Brillouin spectroscopy measurements, six elastic constants (C_{11}, C_{33}, C_{44}, C_{66}, C_{12}, and C_{14}) of a flux-grown GeO_2 single crystal with the α-quartz-like structure are obtained in the 298–1273 K temperature range. High-temperature powder X-ray diffraction data is collected to determine the temperature dependence of the lattice parameters and the volume thermal expansion coefficients. The temperature dependence of the mass density, ρ, is evaluated and used to estimate the thermal dependence of its refractive indices (ordinary and extraordinary), according to the Lorentz–Lorenz equation. The extraction of the ambient piezoelectric stress contribution, e_{11}, from the C'_{11}–C_{11} difference gives, for the piezoelectric strain coefficient d_{11}, a value of 5.7(2) pC N^{-1}, which is more than twice that of α-quartz. As the quartz structure of α-GeO_2 remains stable until melting, piezoelectric activity is observed until 1273 K.

1. Introduction

Under ambient conditions, GeO_2 crystallizes in the rutile structure ($P4_2/mnm$), whereas the α-quartz isotype GeO_2 (α-GeO_2), with the trigonal structure ($P3_121$ or $P3_221$), is stable from 1306 K to its melting point at 1389 K.[1,2] α-GeO_2 is investigated for its potential to replace quartz in some piezoelectric devices. Previous works on the α-quartz-homeotype family show that several properties are linearly linked to their structural distortion.[3] α-GeO_2 presents a highly distorted structure, which prevents the α- to β-quartz phase transition (observed around 846 K in quartz), and should result in an electromechanical coupling coefficient, k, at least twice that of quartz.[3–6]

Growth of large-sized α-GeO_2 single crystals has been demonstrated by using a modified hydrothermal method.[7] Their room temperature infrared (IR) spectra indicated the presence of hydroxyl groups and water molecules incorporated through the aqueous medium. The latter are impurities that catalyze the α-quartz-to-rutile phase transition at temperatures as low as 453 K in GeO_2 single crystals.[7] Furthermore, OH groups act as structural defects and tend to decrease the piezoelectric properties of the material as a function of temperature.

Millimeter-sized OH-free GeO_2 single crystals have successfully been synthesized by using the high-temperature solution method.[6,8] Vibration bands of hydroxyl groups or water molecules were not detected by transmission IR spectroscopy in these flux-grown α-GeO_2 materials. Accordingly, no phase transition was detectable through differential scanning calorimetry (DSC) until melting occurred. The high thermal structure stability until 1273 K was also confirmed by using Raman spectroscopy and powder X-ray diffraction (XRD) data.[5,6] These preliminary results confirmed the high potential of flux-grown α-GeO_2-based single crystals as piezoelectric materials for high-temperature applications. In this context, their physical-property characterizations need to be extended to their elastic behavior as a function of temperature under atmospheric pressure.

A set of elastic constants (C_{ij}), at constant electric displacement and ambient conditions, has already been reported for hydrothermally grown α-GeO_2.[9,10] However, data concerning their thermal evolution are, to the best of our knowledge, not available.

This paper reports on the first Brillouin scattering study of flux-grown α-GeO_2 single crystals from room temperature to 1273 K. The thermal evolution of the elastic constants is discussed and compared with previous reports on materials of the same α-quartz family. Accurate determination of elastic constants from Brillouin scattering depends on two temperature-sensitive physical parameters: refractive index (the ordinary, n_o, and the extraordinary, n_e, indices for a uniaxial crystal)

[a] Dr. A. Lignie, Dr. P. Armand, Dr. P. Hermet, Prof. P. Papet
Institut Charles Gerhardt Montpellier
UMR 5253, CNRS-UM2-ENSCM-UM1, C2M
Université Montpellier 2, CC 1504
Place Eugène Bataillon, 34095 Montpellier Cédex 5 (France)
Fax: (+33) 467144290
E-mail: Pascale.Armand@univ-montp2.fr

[b] Dr. W. Zhou, Dr. B. Rufflé
Institut Charles Coulomb
UMR 5221 CNRS-UM2, Université Montpellier 2, CC 069
Place Eugène Bataillon, 34095 Montpellier Cédex 5 (France)

[c] J. Debray, Dr. B. Ménaert
Institut Néel, Dpt. Matière Condensée, Matériaux et Fonctions
25 avenue des Martyrs, Bâtiment F, BP 166
38042 Grenoble Cédex 9 (France)

[d] R. Mayet, Dr. P. Thomas
Science des Procédés Céramiques et de Traitements de Surface
Centre Européen de la Céramique, UMR 6638
12 Rue Atlantis, 87068 Limoges Cédex (France)

Supporting Information for this article is available on the WWW under http://dx.doi.org/10.1002/cphc.201300793.

and the mass density, ρ. The temperature dependence of ρ, extracted from high-temperature powder XRD (HTPXRD), was used to obtain the thermal evolution of the refractive indices of α-GeO_2 by using the Lorentz–Lorenz equation.

2. Results

2.1. Acoustic-Mode Frequencies

The crystallographic orientations of the different plates, obtained by polishing the as-grown GeO_2 single crystals, were checked by using conoscopy. The Friedel's interference pattern depends on the crystallographic face. For example, Figure 1a shows a cross-interference pattern, which is characteristic of a uniaxial sample. For trigonal samples, this is consistent with a *Z*-face normal to the optical axis corresponding to the helical axis. The *Y*-plate, Figure 1b, presents the interference pattern of a face parallel to the optical axis. The measured disorientation, owing to the polishing, did not exceed 0.2–0.3°.

For materials with the trigonal structure, Brillouin scattering from an X-plate only shows a longitudinal acoustic mode, denoted herein as γ_1. α-GeO_2 is a uniaxial material with optical birefringence. Owing to this property, the Brillouin frequency shift of the γ_1 mode depends on the polarization direction of the incident laser light. The temperature dependence of the Brillouin frequency shift associated with n_e for the γ_1 mode was measured as a function of the temperature, from room temperature to 1273 K (Figure 2a). The signal intensity of this mode was very strong compared to the intensity of the residual elastic peak.

In contrast, the signal intensity of the transverse acoustic mode, denoted γ_4 (Figure 2d), of the α-GeO_2 Y-plate was very weak. From the α-GeO_2 *Y*-plate, a pseudo-longitudinal γ_2 (Figure 2b) and a pseudo-transverse γ_3 acoustic wave (Figure 2c) also registered from 298 to 1273 K, whereas a longitudinal and a transverse acoustic wave, respectively denoted γ_5 and γ_6 (Figure 2e and f), were measured as a function of temperature with the α-GeO_2 *Z*-plate.

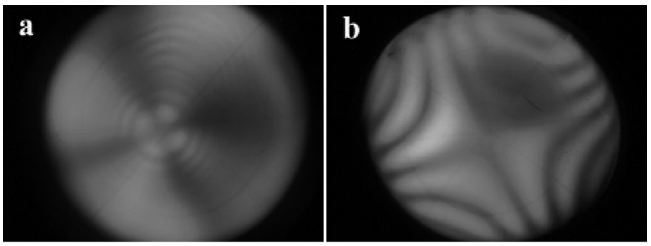

Figure 1. Conoscopy images of a α-GeO_2 *Z*-plate (left) and *Y*-plate (right).

The temperature dependence of these six acoustic modes is plotted in Figure 3 (polynomial parameters available in the

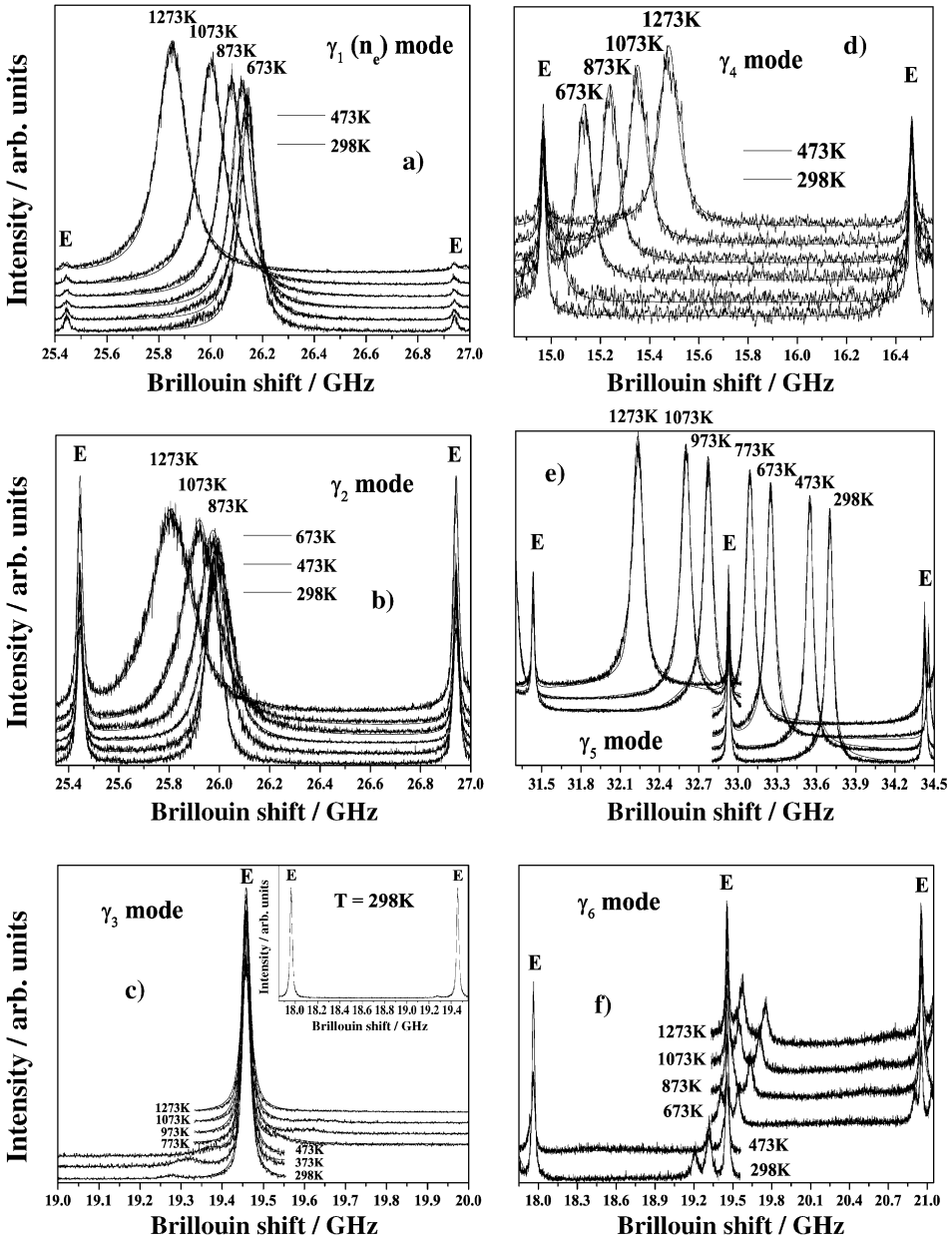

Figure 2. Thermal evolution of different acoustic modes: a) γ_1, b) γ_2, c) γ_3, d) γ_4, e) γ_5, and f) γ_6. Elastic peaks, identified by the letter E, and Brillouin lines are observed at different interference orders.

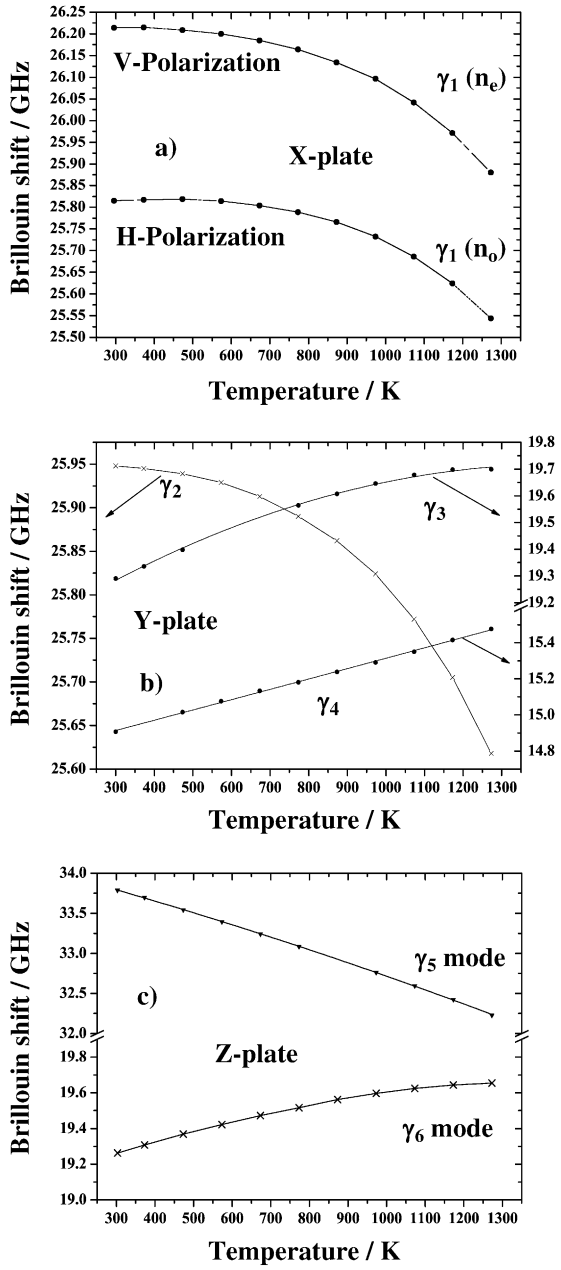

Figure 3. Thermal dependence of a) the longitudinal acoustic mode γ_1 (α-GeO_2 *X*-plate), b) the pseudo-longitudinal acoustic mode (γ_2), the pseudo-transverse acoustic mode (γ_3), and the transverse acoustic mode (γ_4) of the α-GeO_2 *Y*-plate, and c) the longitudinal acoustic mode (γ_5) and the transverse acoustic mode (γ_6) of the α-GeO_2 *Z*-plate.

Supporting Information). Upon increasing the temperature, some modes cross the elastic peak signal, preventing their measurement (γ_4 mode at 400 K, γ_3 mode at 600 and 700 K, and γ_5 mode at 900 K).

2.2. HTPXRD Experiments

Figure 4 shows the XRD patterns of flux-grown α-GeO_2 registered at several temperatures from room temperature to 1323 K. Their comparison shows that the overall XRD patterns remain the same from room temperature to 1323 K. All the diffraction peaks could be assigned to the α-quartz phase of GeO_2. No secondary phase, such as the GeO_2 rutile-like phase or flux phase, could be detected.

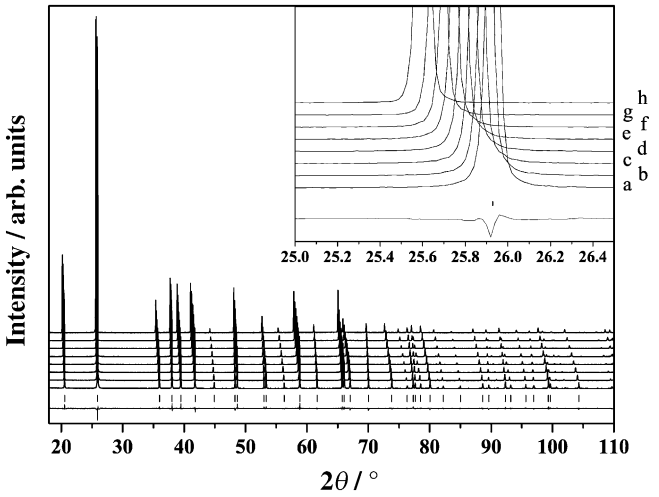

Figure 4. Diffractograms of α-GeO_2 at a) room temperature, b) 423, c) 573, d) 723, e) 873, f) 1023, g) 1173, and h) 1323 K.

Lattice parameters (*a* and *c*) and the unit-cell volume (*V*), detailed in Table 1, were extracted from HTPXRD diffractograms by using the LeBail method implemented in Fullprof software.[11,12]

The mean linear thermal coefficients of the lattice parameters in the temperature range 298–1323 K were calculated according to Equation (1):

$$\overline{\alpha_{(X)}} = \frac{1}{X_{298}} \frac{X_{1323} - X_{298}}{1323 - 298} \quad (1)$$

in which *X* represents the lattice parameter *a* or *c*. $\overline{\alpha_{(a)}}$ and $\overline{\alpha_{(c)}}$ of flux-grown α-GeO_2, $1.60 \times 10^{-5}\,K^{-1}$ and $3.08 \times 10^{-6}\,K^{-1}$ respectively, are close to previously reported values for commercial α-GeO_2 powder.[13] The large difference between $\overline{\alpha_{(a)}}$ and $\overline{\alpha_{(c)}}$ describes the preferential expansion of α-GeO_2 along the *a* axis.

The mass density, ρ, of flux-grown α-GeO_2 was calculated as a function of temperature, Table 1, by using Equation (2):

$$\rho(T) = \frac{Z \times M}{N_a \times V(T)} \quad (2)$$

in which *Z* is the number of formulas per unit cell ($Z = 3$), *M* is the molecular mass ($M = 104.6\ g\,mol^{-1}$), and N_a is Avogadro's number ($6.022 \times 10^{23}\ mol^{-1}$).

2.3. Determination of Refractive Indices

The measurements of the n_e and n_o refractive indices at room temperature for the α-GeO_2 crystal were performed by using the ellipsometry method, which resulted in $n_e = 1.677$ and $n_o = 1.651$ (details concerning the calculation of these values can

Table 1. Crystallographic results and reliability factors extracted from LeBail refinements of α-GeO_2 patterns recorded at different temperatures. The corresponding mass density, ρ, and refractive indices, n_o and n_e, calculated at each measured temperature are also presented. Standard deviations are given in parentheses.

T [K]	a [Å]	c [Å]	V [Å^3]	Rp[a]	Rwp[b]	Rexp[c]	χ^{2}[d]	ρ [g cm^{-3}]	n_o	n_e
298	4.98464(3)	5.64753(4)	121.523(1)	6.71	10.4	7.21	2.07	4.2875(3)	1.6510	1.6771
423	4.99262(3)	5.64896(4)	121.943(1)	3.36	10.1	7.07	2.05	4.2727(2)	1.6480	1.6739
573	5.00332(3)	5.65144(4)	122.520(1)	6.14	9.81	7.07	1.93	4.2526(3)	1.6442	1.6699
723	5.01456(4)	5.65411(5)	123.129(2)	6.62	12.5	7.14	3.07	4.2316(3)	1.6402	1.6657
873	5.02631(4)	5.65701(5)	123.770(2)	7.21	12.5	7.17	3.06	4.2096(3)	1.6360	1.6613
1023	5.03885(4)	5.65989(5)	124.452(2)	7.36	11.7	7.13	2.71	4.1866(3)	1.6317	1.6567
1173	5.05221(5)	5.66286(6)	125.178(2)	7.92	13.3	7.23	3.41	4.1623(3)	1.6271	1.6519
1323	5.06633(4)	5.66538(4)	125.935(2)	7.46	11.4	7.19	2.53	4.1373(3)	1.6224	1.6469

[a] $Rp = 100 \times \sum(|Fo - Fc|)/\sum Fo$, [b] $Rwp = 100 \times \sqrt{\sum |Fo - Fc|^2 / \sum |Fo|^2}$, [c] $Rexp = 100 \times \sqrt{[(N - P + C)/\sum (wF_0^2)]}$, and [d] $\chi^2 = 100 \times (Rwp/Rexp)$. N is the number of measurements in the diffractogram, P is the total number of refined parameters, C is the number of constraints, w is the weigthing factor [$w = 1$/variance (Fo)], Fo is the observed intensity, and Fc is the calculated intensity.

be found in ref. [14]). The n_o index value is in agreement with that reported by Grimsditch et al. ($n_o = 1.65$).[10]

The thermal dependence of the ratio n_e/n_o was obtained from the ratio between the Brillouin frequency shifts associated to $\gamma_1(n_e)$ and $\gamma_1(n_o)$. The behavior of this ratio with temperature (in Kelvin) was fitted to a second-order polynomial law [Eq. (3)]:

$$\frac{n_e}{n_0}(T) = 1.016(2) - 1.1(3) \times 10^{-6}\, T - 7.8(2) \times 10^{-10}\, T^2 \qquad (3)$$

To estimate the variation of the refractive indices n_e and n_o of α-GeO_2 as a function of temperature, the modified Lorentz–Lorenz formula was used [Eq. (4)]:

$$\frac{n_{j(T)}^2 - 1}{\left\langle n_{(T)}^2 \right\rangle + 2} * \frac{1}{\rho(T)} = k \quad (n_j = n_o \text{ or } n_e) \qquad (4)$$

in which k does not depend on T and $\left\langle n_{(T)}^2 \right\rangle = \left(n_e^2 + 2\, n_0^2\right)/3$ is the average value of the refractive indices.

By using the room-temperature values of refractive indices and mass density [4.2875(3) g cm^{-3}], k was first calculated for each refractive index, n_o and n_e, as being 0.0847 and 0.0889 cm^3 g^{-1}, respectively, at 298 K. The thermal variation of the refractive indices was then determined from the thermal evolution of the mass density. The thermal dependence of the flux-grown α-GeO_2 mass density from room temperature to 1323 K (see values in Table 1) was fitted by using a second-order polynomial law [Eq. (5)], with T in Kelvin, as shown in Figure 5a.

$$\rho(T) = 4.2914(3) - 1.22(1) \times 10^{-4}\, T - 2.36(2) \times 10^{-8}\, T^2 \qquad (5)$$

The mass density values at several temperatures were obtained by using Equation (5) and the values of n_o and n_e at $\lambda = 514.5$ nm were deduced from Equation (4) for all the studied temperatures (see Table 1). Their dependence on temperature was plotted, Figure 5b, and fitted with a second-order polynomial law as reported [Eqs. (6) and (7)]:

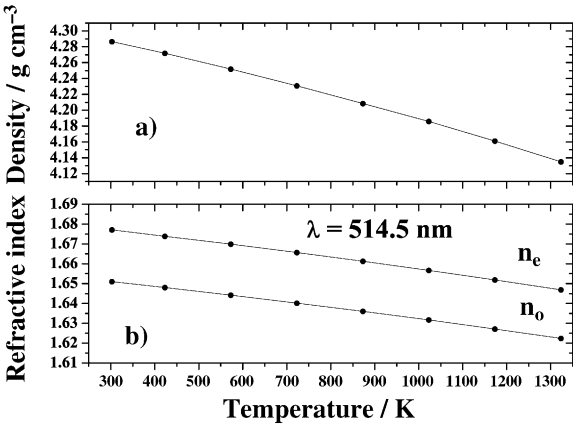

Figure 5. a) Refractive indices at $\lambda = 514.5$ nm and b) density of α-GeO_2 with temperature. Error bars are smaller than the symbol size.

$$n_o^{514.5\,nm}(T) = 1.6577(1) - 2(2) \times 10^{-5}\, T - 4.18(1) \times 10^{-9}\, T^2 \qquad (6)$$

$$n_e^{514.5\,nm}(T) = 1.6841(1) - 1(2) \times 10^{-5}\, T - 4.51(8) \times 10^{-9}\, T^2 \qquad (7)$$

3. Discussion

3.1. Acoustic-Mode Frequencies

It is important to emphasize that the same *Y*-plate was used to determine the temperature dependence of acoustic modes γ_2 to γ_4, and the same *Z*-plate was used to identify that of the γ_5 and γ_6 acoustic modes. These flux-grown α-GeO_2 samples were heated to 1273 K several times without presenting the well-known milky hue (opaque) that reduces the piezoelectric quality of α-quartz-like crystals, obtained by the hydrothermal method, at high temperature.[15] This effect has been attributed to the release of water from hydroxyl impurities with increasing temperature.

Furthermore, the thermal behavior of the flux-grown plates differs from that of reflux-grown materials, as we did not observed any α-quartz↔rutile phase transition.[6,7] This improved thermal stability range of α-GeO_2 can be related to the negligi-

ble OH content in flux-grown single crystals and explains why the plates were not affected by successive thermal cycles from 303 to 1273 K.[6]

The high resolution of the Brillouin spectrometer enabled us to reveal the lifting of the degeneracy of the shear-wave velocity of the γ_6 mode, a manifestation of the so-called acoustical activity (a mechanical analogue of optical activity). This effect has been predicted to exist in the case of propagation along high-symmetry axes (3-fold or higher symmetry), as in the case of optical activity, as a simple rotation of the plane of polarization of transverse acoustic modes.[16] The shear-wave doublet was registered with the α-GeO_2 Z-plate in function of temperature, Figure 2 f. The Brillouin shift, amplitude, and width of the acoustical vibration modes were obtained by least-squares fits to the spectra. The standard errors, given by the routine calculation (variance analysis), provide estimations of the Brillouin-shift errors, which are below 0.01 GHz for all the modes. At ambient temperature, the measured doublet splitting, $\delta\Delta_{\nu_R}$, is 110 MHz for a mean phonon frequency $\overline{\Delta\nu_B} = 19.27$ GHz. The gyrotropic constant of the α-GeO_2 material, given by $\gamma = \delta\Delta_{\nu_R}/\overline{\Delta\nu_B}^{-2}$, was found to be 2.96×10^{-4} GHz^{-1}, which is equivalent to that of α-quartz, $\gamma = 3.0\times10^{-4}$ GHz^{-1}.[17] A previous Brillouin study on $GaPO_4$ flux-grown single crystals with the α-quartz structure reported a value of 2.2×10^{-4} GHz^{-1}.[18]

The acoustic gyrotropic tensor is a fifth-rank tensor characterized by $d_{ij,l} = -d_{ji,l}$ (using Voigt notation), which controls the acoustical activity. By using group theoretical methods, the number of independent coefficients of this tensor could be reduced.[16] For α-GeO_2, the value of the $d_{54,3}$ acoustic gyrotropic tensor, given by $d_{54,3} = (\lambda\ \delta\Delta_{\nu_R}C_{44})/(4\pi n_o\Delta\nu_B)$ is 5.42 N m^{-1}. It evolves greatly with temperature, reaching 9.48 N m^{-1} at 1273 K. These values could be of importance for the realization of gyrotropic waveguides.[19] Compared to the room-temperature $d_{54,3}$ coefficients of α-$GaPO_4$ and α-SiO_2 (4.4 N m^{-1} and 13.4 N m^{-1}, respectively), the α-GeO_2 acoustic gyrotropic tensor value is close to that of α-$GaPO_4$, as they show similar relative splitting and C_{44} elastic constant values.[18]

3.2. Room-Temperature Elastic Constants

From the Brillouin spectra recorded at ambient temperature and the refractive indices measured by ellipsometry, we calculated the sound velocities of the six acoustic modes recorded (see the Experimental Section and Table 2). The uncertainty on the velocity was estimated to be in the order of 1–3 m s^{-1}, considering the weak crystallographic deviation and a Brillouin-shift error evaluated below 0.01 GHz for all the modes.

Table 2. Room-temperature Brillouin shifts, ν_B, and sound velocities, v, measured on several α-GeO_2 plates.

Mode	ν_B ($T = 300$ K) [GHz]	v [m s^{-1}]
γ_1	26.214(10)	4021(2)
γ_2	25.974(10)	3984(2)
γ_3	19.290(10)	3005(2)
γ_4	14.907(10)	2304(2)
γ_5	33.788 (10)	5264(2)
γ_6	19.262(10)	3001(2)

By using Voigt's notation and taking into account the crystal symmetry, the α-quartz structure (point group 32) presents six independent elastic moduli: C_{11}, C_{33}, C_{44}, C_{12}, C_{13}, and C_{14} ($2C_{66} = C_{11} - C_{12}$). In the case of piezoelectric material, the expression of the elastic moduli at constant electric field depends on the orientation of the sample. The relative small size of the spontaneously nucleated flux-grown GeO_2 single crystals did not allow us to prepare platelets with the appropriate orientations needed to determine C_{13}. Table 3 presents the expressions of the elastic moduli, C_{ij}, corresponding to the measured acoustic modes from *X*-, *Y*-, and *Z*-oriented plates of our samples.

Table 3. Expression of the eigenvalues, $C^{(s)}$, depending on the registered acoustic mode.

Mode	Geometry	Mode type	Expression of $C^{(s)}$
γ_1	*X*-plate	L[a]	$C_{11} + \frac{e_{11}^2}{\varepsilon_{11}}$
γ_2	*Y*-plate	PL[b]	$\frac{C_{11}+C_{44}}{2} + \frac{\sqrt{(C_{44}-C_{11})^2+4C_{14}^2}}{2}$
γ_3	*Y*-plate	PT[c]	$\frac{C_{11}+C_{44}}{2} - \frac{\sqrt{(C_{44}-C_{11})^2+4C_{14}^2}}{2}$
γ_4	*Y*-plate	T[d]	$C_{66} + \frac{e_{11}^2}{\varepsilon_{11}}$
γ_5	*Z*-plate	L[a]	C_{33}
γ_6	*Z*-plate	T[d]	C_{44}

[a] L = longitudinal. [b] PL = pseudo-longitudinal. [c] PT = pseudo-transverse. [d] T = transverse.

The room-temperature values of the elastic constants C_{ij} (GPa) of flux-grown α-GeO_2 are presented in Table 4. C'_{ij} are elastic constants at constant electric displacement, that is, not corrected from the piezoelectric effect $e_{11}^2/\varepsilon_{11}$, in which e_{11} is the piezoelectric stress constant and ε_{11} is the dielectric constant.

The values of the elastic moduli measured for the α-GeO_2 crystal synthesized by using the modified hydrothermal method are very similar to our values, see Table 4.[8] There is a scatter in the values of C_{11} and C_{12}, which are larger (by around 10%) for our flux-grown sample. The origin of the differences between these two C_{ij} constants can be directly attrib-

Table 4. Elastic constants and piezoelectric coefficient of α-GeO_2 and α-SiO_2.

Elastic Constant	GeO_2 ref. [8]	GeO_2 theoretical[a]	GeO_2 this work	SiO_2 ref. [10]
C_{11}	–	62.9	68.1(1)	87
C'_{11}	64	–	69.3(1)	–
C_{12}	22	25.5	25.1(1)	7
C_{13}	32	25.7	–	13
$\lvert C_{14}\rvert$	≈ 0	0.6	≈ 0	18
C_{33}	118	116.8	118.8(2)	107
C_{44}	38	35.0	38.6(1)	57
C_{66}	–	18.7	21.5(1)	40
C'_{66}	21	–	22.7(1)	–
d_{11} (10^{-12} C N^{-1})	4.04[b]	7.434	5.7(2)	2.31[b]

[a] $T = 0$ K. [b] See ref. [8].

uted to the crystal quality, which is related to the growth technique used to obtain the α-GeO_2 single crystals. The presence of hydroxyl groups and water molecules were reported for hydrothermally grown GeO_2 single crystals, whereas OH-free α-GeO_2 crystals were grown with the flux technique.[7,8] In general, the elastic behavior of a solid depends on its atomic structural arrangement and on the strength of its interatomic binding forces.[20] Thus, the presence of OH-interactions in the crystal would increase its ionic character and, consequently, soften its elastic behavior. These OH impurities would mainly affect C_{11} and C_{12}, which characterize elongation in the (*XY*) plane to normal and a shear stress, respectively. This suggests a preferential distribution of OH defects along the *X*-axis in α-GeO_2, as observed in isostructural compounds such as α-SiO_2 and α-$GaPO_4$.[21–24]

Our room-temperature experimental C_{ij} values show good agreement with computed values at 0 K (Table 4). The largest discrepancy was observed for C_{66} (almost 13% softer for the theoretical value), whereas a good accordance was found for the C_{12} and C_{14} elastic constants.

The room-temperature value of the piezoelectrically stiffened C'_{11} elastic constant, presented in Table 4, was obtained from the longitudinal acoustic mode γ_1 of the flux-grown α-GeO_2 *X*-plate, whereas the pure C_{11} elastic constant was deduced from the sum of the pseudo-longitudinal γ_2 and the pseudo-transverse γ_3 modes of the *Y*-plate, subtracted by the C_{44} value deduced from the γ_6 mode measured on the *Z*-plate, see Table 3. The difference $C'_{11}-C_{11}$ allows us to deduce the numerical value of the piezoelectric term $e_{11}^2/\varepsilon_{11}$ as 1.29(2) GPa at room temperature. For the flux-grown α-GeO_2 crystal, a value of $4.8(9)\times10^{-11}$ F m^{-1} was measured for its dielectric constant ε_{11} at 1 kHz and at ambient temperature on an *X*-oriented plate. By using this value, we can deduce a piezoelectric stress constant, e_{11}, of 0.24(1) C m^{-2}, according to Equation (8):

$$e_{11} = d_{11} \times (2\,C_{66}) + d_{14} \times C_{14} \quad (8)$$

C_{14} is approximately equal to zero; therefore, we can approximate a d_{11} piezoelectric strain constant of $5.7(2)\times10^{-12}$ C N^{-1} for the flux-grown α-GeO_2 material, which is close to the value of 6.00×10^{-12} C N^{-1} that was predicted by Krempl.[25] This approximate d_{11} piezoelectric constant value lies between that calculated at 0 K and the reported room-temperature experimental value from the hydrothermally grown GeO_2 compound (Table 4). Again, the large discrepancy between the two experimental α-GeO_2 d_{11} values reported in Table 4 can be attributed to a better crystal quality of the water-free flux-grown α-GeO_2 crystals.[4,6]

The flux-grown α-GeO_2 crystal exhibits an approximate d_{11} piezoelectric strain constant that is more than twice that of α-quartz SiO_2 (Table 4), confirming the improvement of the piezoelectric properties with the structural distortion, as indicated by Philippot et al.[3]

3.3. Temperature Dependence of the Elastic Constants

The temperature dependence of the elastic moduli C_{ij} of α-GeO_2 from room temperature to 1273 K is presented in Figure 6a–c. Some of the missing Brillouin frequency shifts were estimated by using a second-order polynomial interpolation (polynomial parameters available in supporting information). The C_{11}, C_{33}, and C_{12} elastic constants show monotonic elastic softening upon heating (Figure 6b and c), whereas C_{44} and C_{66} show continuous stiffening (Figure 6a). Most C_{ij} values change by only a few percent, whereas C_{12} decreases by about 21%. The elastic constants measured in the 298–1273 K temperature range are in agreement with the conservation of the α-quartz structure of GeO_2 flux-grown material with temperature demonstrated by the HTPXRD experiment.

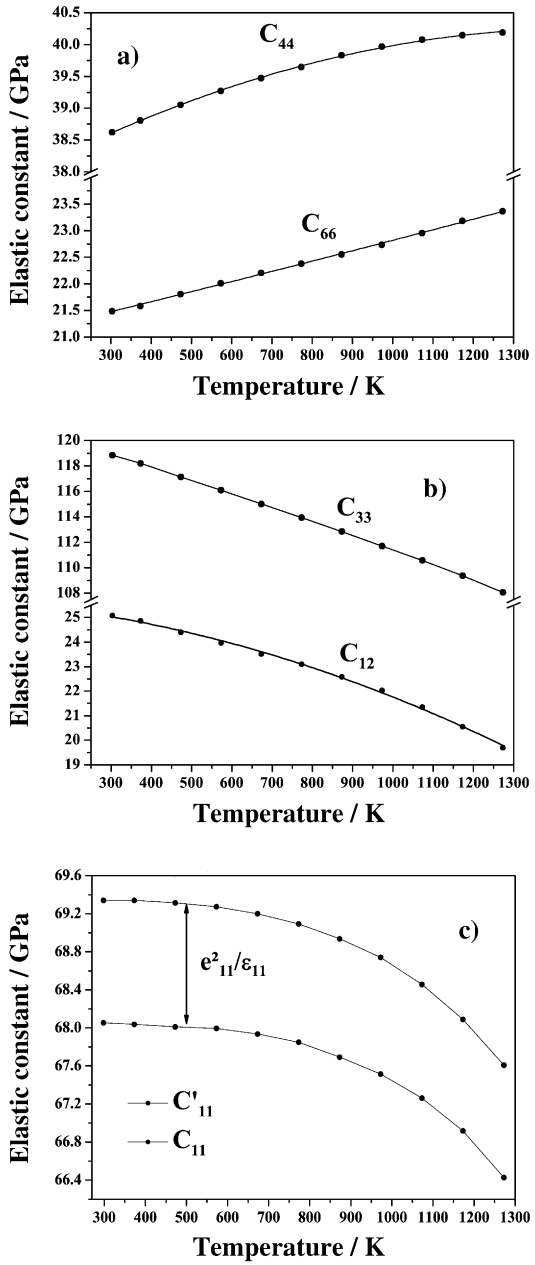

Figure 6. Thermal dependence of a) the C_{44} and C_{66} elastic constants, b) the C_{33} and C_{12} elastic constants, and c) the C_{11} elastic constant (pure and piezoelectrically stiffened) of GeO_2. The difference between those curves gives the value of the piezoelectric contribution. Errors are smaller than the symbol size.

The superposition of the thermal evolution of the C'_{11} and C_{11} elastic constants in Figure 6c permits direct visualization of the thermal evolution of the piezoelectric term $e_{11}^2/\varepsilon_{11}$, which remains stable until 1273 K. The flux-grown α-GeO_2 sample still exhibits a piezoelectric activity at high temperature; therefore, it could be a promising material for high-temperature piezoelectric devices. Moreover, it is important to recall that the α-GeO_2 plates were heated several times at high temperature (1273 K) without losing their high visual transparency.

Owing to the relatively small dimension of our α-GeO_2 *X*-plate (a few millimeters in length), we were not able to measure the thermal evolution of the ε_{11} dielectric constant with enough precision to deduce that of the e_{11} piezoelectric constant.

4. Conclusions

In this Brillouin scattering study, we demonstrated the analysis of elastic properties of flux-grown GeO_2 single crystals, which adopted the α-quartz structure, over a wide temperature range (300–1273 K).

At ambient temperature, the elastic constants values of the flux-grown α-GeO_2 samples presented close similarities with those published on hydrothermally grown materials. Therefore, compared with hydrothermally grown α-GeO_2 crystals, the strong reduction in OH concentration in the lattice of our samples is believed to have induced a slightly stiffer behavior. The higher crystal quality of our samples was also reflected by the conservation of their high visual transparency and the preservation of the α-quartz structure after several heat treatments. The evolution of five out of the six independent elastic constants of α-GeO_2 with temperature showed that expected for the pure shear C_{44} and C_{66} elastic constants; a softening of the elastic moduli occurred with temperature because of thermal expansion.

The potential of a α-GeO_2 single crystal for the realization of piezoelectric devices was also confirmed, as its d_{11} piezoelectric constant at ambient temperature was found to be more than twice that of α-quartz. The piezoelectric property of α-GeO_2 was maintained at high temperature, as a significant piezoelectric contribution to C_{11} still existed at 1273 K.

Centimeter-sized α-GeO_2 *X*- and *Y*-plates could be grown to precisely measure their piezoelectric properties as a function of temperature by using resonant methods and confirm the relevancy of GeO_2 as a material for high-temperature piezoelectric devices.

Experimental Section

Syntheses and Realization of Oriented Plates

As described in details in ref. [6], transparent, well-facetted, and millimeter-sized single crystals of GeO_2 were grown by spontaneous nucleation with a high-temperature flux-growth process by using the slow-cooling method. Oriented platelets were cut and polished from as-grown samples presenting no visible imperfections such as trapped gas-bubbles or flux inclusions.

To identify the crystalline orientation, we used the dielectric system, also known as the orthogonal system. In this system, the *Z*-axis of α-GeO_2 coincided with the crystallographic *c*-axis; the *X*-axis matched the crystallographic *a*-axis, and the *Y*-axis was normal to the *X*- and *Z*-axes (with the *b*-axis in the *XY* plane at 120° from the *a*-axis). The average size of the flux-grown GeO_2 single crystals, 3–5 mm in length, allowed us to prepare plates with simple orientations. Three platelets were obtained, defined in the orthogonal system as *X*-plate, *Y*-plate, and *Z*-plate, which corresponded to the (10.0), (2–1.0), and (00.3) *hkl*-crystallographic planes, respectively.

As for α-quartz, there is a possibility of the existence of optical and electrical twins in these α-GeO_2 plates. However, following the procedure described in ref. [4], we were able to determine that no Brazil (optical) twins were present in the measured samples.

Characterization

Brillouin scattering is caused by the inelastic interaction of an incident photon with acoustic phonons of the medium. It results in a frequency shift, $\pm\Delta\nu_B$, of the scattered light relative to the laser frequency, depending on its velocity of propagation and, hence, on the elastic tensor, C_{ijkl}, of the medium. For piezoelectric media, such as α-GeO_2, a stress component is also produced by the internal electric field, *E*, so that the usual relationship between the stress tensor, T_{ij}, and the strain tensor, S_{kl}, is modified according to Equation (9):[26]

$$T_{ij} = C_{ijkl}S_{kl} - e_{mij}E_m \tag{9}$$

in which *e* is the piezoelectric tensor and summation over repeated indices is implied. For long waves, it can be shown that it results in an effective elastic tensor, $C^{(e)}$, that depends on the propagation direction [Eq. (10)]:

$$\left| C_{ijkl}^{(e)} + \frac{e_{mij}e_{nkl}\hat{Q}_m\hat{Q}_n}{\varepsilon_{gh}\hat{Q}_g\hat{Q}_h} - C\delta_{ik} \right| = 0 \tag{10}$$

in which ε is the dielectric tensor at the frequency of the elastic wave. For the propagation direction, $\hat{Q}$, the three eigenvalues of $C^{(s)}$ are given by the usual Christoffel matrix [Eq. (11)]:

$$\left| C_{ijkl}^{(e)}\hat{Q}_j\hat{Q}_l - C\delta_{ik} \right| = 0 \tag{11}$$

in which δ_{ik} is the unit tensor.

These eigenvalues, $C^{(s)}$, are associated to a phase velocity, $v^{(s)}$, of the sound wave according to Equation (12):

$$v^{(s)} = \sqrt{C^{(s)}/\rho} \tag{12}$$

in which ρ is the material mass density.

Finally, the Brillouin frequency shift measured in the backscattering geometry are related to the sound velocity through Equation (13):

$$\Delta\nu_B = \frac{(n_i + n_s)v}{\lambda} \tag{13}$$

in which λ is the wavelength of the incident laser light, n_i and n_s are the refractive indices of the crystal for incident and scattered light, respectively.

More details concerning this technique and the different relationships established between the frequency shift, the density, and the wavelength of the incident wave, according to the propagation vector, can be found elsewhere.[26–28]

A high-resolution Brillouin spectrometer (resolving power of about 10^7) operating with an Ar-laser ($\lambda = 514.5$ nm) was used in the backscattering geometry to measure the sound velocities necessary to determine the elastic constant. The spectrometer was composed of a fixed planar Fabry–Perot (FP) interferometer [1.5 mm spacing, free spectral range (FSR) of ca. 100 GHz, resolution ca. 1.7 GHz full-width at half-maximum (FWHM)], working as a band-pass filter. The thickness and the parallelism of this FP were dynamically adjusted to maximize the transmission of one of the two Brillouin lines of the acoustic mode under study. To that effect, an electro-optically modulated signal at the Brillouin frequency shift was periodically sent into the spectrometer. The high-resolution Brillouin spectrum was obtained by scanning a thick confocal FP interferometer (25 mm spacing, FSR ca. 3 GHz, resolution ca. 60 MHz at FWHM) placed after the planar FP. A detailed description of the apparatus and its principles can be found elsewhere.[29,30] According to the narrow band-pass of the first FP, only one acoustic mode was generally recorded at a time with this set-up.

The backscattered signal from the sample was collected by a short-focal-length lens ($f = 25$ mm) through a numerical aperture (NA) of approximately 0.18 and sent to the Brillouin spectrometer. The finite aperture-induced Brillouin frequency downshift was taken into account in the data analysis, assuming an isotropic sound velocity in the probed $\vec{q}$-region. The single-crystals were mounted on a Linkam TS 1500 heating stage and heated in air from ambient temperature to 1273 K, with a heating rate of 20 K min^{-1}. The measurements were started after a waiting time of 300 s, ensuring thermal equilibrium. Approximately 30 scans, corresponding to an acquisition time of approximately 8 min, were needed to achieve sufficient statistics. After cooling to room temperature, it was systematically verified that the room-temperature Brillouin frequency shift was recovered.

High-temperature XRD was performed on a D8 Avance diffractometer (Bruker) equipped with a Ge monochromator [crystallographic plane (111)] and working with the CuKα_1 radiation ($\lambda = 1.54059$ Å). Samples, sieved to 20 μm, were placed on a platinum surface in an HTK 1200N oven (Anton Paar) and heated to around 1323 K in air, with temperature steps of 100 K. The thermal expansion of the platinum plate was automatically compensated. The temperature ramp was 10 K min^{-1} (heating) or 30 K min^{-1} (cooling). Temperatures were fixed for at least 600 s before recording the diffractogram from 10° to 110° (2θ values). From the XRD experiments, the temperature dependence of the mass density and the bulk thermal expansion coefficients were deduced.

Conoscopy figures were recorded on a polarizing microscope composed of two crossed-polarizing filters (polarizer and analyzer) into the optical path. The refractive indices were measured on a SOPRA GES5E spectroscopic ellipsometer equipped with a xenon lamp. The measurements were made at $\lambda = 514.5$ nm on a α-GeO_2 *Y*-plate. Two orientations (*Z*-axis of the *Y*-plate placed parallel or perpendicular to the polarization of the electric field) were used to deduce both extraordinary and ordinary refractive indices.

Computed C_{ij} values were calculated within the density functional theory framework, as implemented in the ABINIT package.[31] Details about the computation of the elastic, piezoelectric, and internal force-response tensors can be found in ref. [32]. The exchange-correlation energy functional was evaluated within the local density approximation (LDA) as proposed by Perdew and Wang.[33] Relaxations of the lattice parameters and the atomic positions were performed by using the Broyden–Fletcher–Goldfarb–Shanno algorithm until the maximum residual forces on the atoms and stress were less than 1×10^{-6} Ha Bohr^{-1} and 1×10^{-4} GPa, respectively. Convergence was reached for a 70 Ha plane-wave kinetic energy cutoff and a $8\times8\times8$ mesh of special *k*-points.[34]

Keywords: Brillouin spectroscopy · elastic constants · germanium oxide · single crystal · X-ray diffraction

[1] V. G. Hill, L. L. Y. Chang, *Am. Mineral.* **1968**, *53*, 1744.
[2] A. Laubengayer, D. S. Morton, *J. Am. Chem. Soc.* **1932**, *54*, 2303.
[3] E. Philippot, D. Palmier, M. Pintard, A. Goiffon, *J. Solid State Chem.* **1996**, *123*, 1.
[4] A. Lignie, D. Granier, P. Armand, J. Haines, P. Papet, *J. Appl. Crystallogr.* **2012**, *45*, 272.
[5] G. Fraysse, A. Lignie, P. Hermet, P. armand, D. Bourgogne, J. Haines, B. Menaert, P. Papet, *Inorg. Chem.* **2013**, *52*, 7271.
[6] A. Lignie, P. Armand, P. Papet, *Inorg. Chem.* **2011**, *50*, 9311.
[7] D. V. Balitsky, V. S. Balitsky, Y. V. Pisarevsky, E. Philippot, O. Y. Silvestrova, D. Y. Pushcharovsky, *Ann. Chim.-Sci. Mater.* **2001**, *26*, 183.
[8] P. Armand, S. Clement, D. Balitsky, A. Lignie, P. Papet, *J. Cryst. Growth* **2011**, *316*, 153.
[9] D. B. Balitskii, O. Y. Silvestrova, V. S. Balitski, Y. V. Pisarevski, D. Y. Pushcharovski, E. Philippot, *Crystallogr. Rep.* **2000**, *45*, 145.
[10] M. Grimsditch, A. Polian, V. Brazhkin, D. Balitskii, *J. Appl. Phys.* **1998**, *83*, 3018.
[11] J. Rodriguez-Carvajal, *J. Phys. B* **1993**, *192*, 55.
[12] T. Roisnel, J. Rodriguez-Carvajal, *Matter. Sci. Forum* **2001**, *378*, 118.
[13] J. Haines, O. Cambon, E. Philippot, L. Chapon, S. Hull, *J. Solid State Chem.* **2002**, *166*, 434.
[14] J. L. Duarte, J. A. Sanjurjo, R. S. Katiyae, *Phys. Rev. B* **1987**, *36*, 3368.
[15] W. Wallnöfer, J. Stadler, P. Krempl, *Proc. 7th Eur. Freq. Time Forum* Neuchâtel Switzerland, **1993**, 653.
[16] D. L. Portigal, E. Burstein, *Phys. Rev.* **1968**, *170*, 673.
[17] A. G. Every, *Phys. Rev. B* **1987**, *36*, 1448.
[18] P. Armand, M. Beaurain, B. Rufflé, B. Ménaert, P. Papet, *Inorg. Chem.* **2009**, *48*, 4988.
[19] A. Erdmann, P. Hertel, H. Dötsch, *Opt. Quantum Electron.* **1994**, *26*, 949.
[20] H. A. A. Sidek, G. A. Saunders, W. Hong, X. Bin, H. Jianru, *Phys. Rev. B* **1987**, *36*, 7612.
[21] E. Marinho, D. Palmier, A. Goiffon, E. Philippot, *J. Mater. Sci.* **1998**, *33*, 2825.
[22] A. Kats, *Philips Res. Rep.* **1962**, *17*, 133.
[23] K. Shinoda, N. Aikawa, *Phys. Chem. Miner.* **1993**, *20*, 308.
[24] S. Suzuki, S. Nakashima, *Phys. Chem. Miner.* **1999**, *26*, 217.
[25] P. W. Krempl, *J. Phys. IV* **2005**, *126*, 95.
[26] R. Vacher, E. Courtens *International Tables for Crystallography, Vol. D*, edited by A. Authier, published by Kluwer Academic Publishers, Dordrecht/Boston/London, **2003**, chap. 2.4, 329.
[27] R. Vacher, L. Boyer, *Phys. Rev. B* **1972**, *6*, 639.
[28] J. G. Dil, *Rep. Prog. Phys.* **1982**, *45*, 285.
[29] R. Vacher, S. Ayrinhac, M. Foret, B. Rufflé, E. Courtens, *Phys. Rev. B* **2006**, *74*, 012203.
[30] H. Sussner, R. Vacher, *Appl. Opt.* **1979**, *18*, 3815.
[31] X. Gonze, B. Amadon, P.-M. Anglade, J.-M. Beuken, F. Bottin, P. Boulanger, F. Bruneval, D. Caliste, R. Caracas, M. Cote, T. Deutsch, L. Genovese, Ph. Ghosez, M. Giantomassi, S. Goedecker, D. R. Hamann, P. Hermet, F. Jollet, G. Jomard, S. Leroux, M. Mancini, S. Mazevet, M. J. T. Oliveira, G. Onida, Y. Pouillon, T. Rangel, G.-M. Rignanese, D. Sangalli, R. Shaltaf, M. Torrent, M. J. Verstraete, G. Zerah, J. W. Zwanziger, *Comput. Phys. Commun.* **2009**, *180*, 2582.
[32] D. R. Hamann, X. Wu, K. M. Rabe, D. Vanderbilt, *Phys. Rev. B* **2005**, *71*, 035117.
[33] J. P. Perdew, Y. Wang, *Phys. Rev. B* **1992**, *45*, 13244.
[34] H. J. Monkhorst, J. D. Pack, *Phys. Rev. B* **1976**, *13*, 5188.

Received: August 27, 2013
Published online on December 2, 2013